Angle-Dependent Carrier Transmission in Graphene p−n Junctions

S. Sutar,*,[†] E. S. Comfort,[†] J. Liu,[†] T. Taniguchi,[‡] K. Watanabe,[‡] and J. U. Lee[†],*

[†]College of Nanoscale Science and Engineering, The State University of New York at Albany, Albany, New York 12203, United States
[‡]National Institute of Materials Science, Tsukuba, Japan

S *Supporting Information*

ABSTRACT: Angle-dependent carrier transmission probability in graphene p-n junctions is investigated. Using electrostatic doping from buried gates, p−n junctions are formed along graphene channels that are patterned to form different angles with the junction. A peak in the junction resistance is observed, which becomes pronounced with angle. This angular dependence is observed for junctions made on both exfoliated and CVD-grown graphene and is consistent with the theoretically predicted dependence of transmission probability on incidence angle.

KEYWORDS: *Graphene, graphene p−n junctions, GPNJ, Klein tunneling, particle chirality, chiral particles*
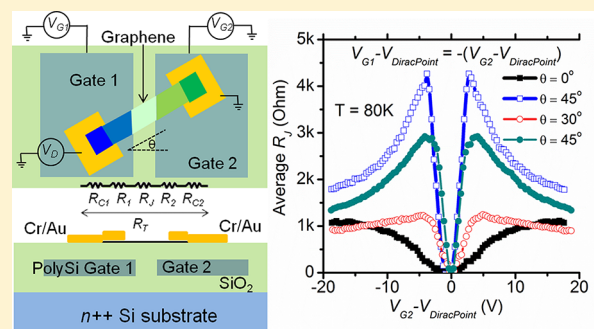
Graphene p−n junctions (GPNJs) are predicted to form a new class of electronic devices that have no analogues in modern electronics. These are based on the remarkable electronic transport properties in graphene[1−5] that lead to angle-dependent transmission in GPNJs in the form of electron focusing in abrupt junctions,[6] and transmission for only near-normal incident carriers in graded junctions.[7,8] This angle-dependent transport has been used to predict novel devices such as the Veselago lens,[6] which is the electronic analogue of a negative index of refraction lens, and is of critical importance in realizing a GPNJ-based low subthreshold swing, high on−off ratio solid state switch for beyond CMOS applications.[9] However, demonstrations of the angular dependence in experiment have been few, notably the reflections of high incidence angle trajectories in p−n electron waveguide[10] and high transmission of normal trajectories in Klein tunneling.[11,12] In this work, we demonstrate the angular dependence of carrier transmission probability in GPNJ, observed from a systematic study of the GPNJ resistance in graphene channels that are tilted relative to the junction. These effects persist up to room temperature and are in agreement with modeling results.

To form p- and n-doped regions, we use electrostatic doping from buried coplanar split gates (SGs) with varying spacing. The SGs were formed by depositing and etching 100 nm of highly doped polysilicon on top of a 100 nm thick thermal oxide. They were patterned to form interdigitated finger structures over a large area, ensuring the placement of exfoliated graphene over these structures. To form the top dielectric, SiO$_2$ was deposited over the SGs and polished using chemical−mechanical-planarization (CMP) to a 100 nm thickness. Here, the CMP process removes any topography associated with the patterned polysilicon SGs and achieves atomically flat surfaces, which we verified with atomic force microscopy (AFM). This process is critical to the formation of p−n junctions that preserves the intrinsic electronic structure of graphene. Next, a reactive ion etch was used to etch the SiO$_2$ over contact pads to expose the underlying SG. Onto the planarized SiO$_2$ surface, graphene was deposited by either mechanically exfoliating graphenium flakes using Scotch tape (3M technologies) or by transferring CVD-grown graphene grown by methods that yield large grains.[13] For both graphene types, we used Raman spectroscopy to confirm that we were indeed measuring the properties of single-layer graphene films. Graphene contact leads in a two-terminal configuration were made by e-beam lithography, followed by metallization with either Cr/Au or Ti/Au (10/50 nm). The contacts were placed close to the junction to minimize parasitic resistances. In Figure 1a, we show the schematic of a junction forming an angle θ with respect to the SG. A number of such junctions were fabricated by patterning and etching graphene at different angles. All devices showed symmetric resistance with doping about the minimum conductivity point (MCP) or the Dirac point (DP). To determine the parameters that influence the junction resistance, we examined junctions with SG spacings of 100, 150, or 200 nm and with alternate substrates, including exfoliated hexagonal boron nitride (hBN) flakes (50 to 150 nm thick, verified using AFM) on top of SiO$_2$ to improve the graphene mobility.[14,15] To remove any possible process variations between junctions, we compared junctions within the same flake for exfoliated graphene or well within the expected grain size of CVD graphene. Figure 1b shows a scanning electron microscope (SEM) image of a SG cross-
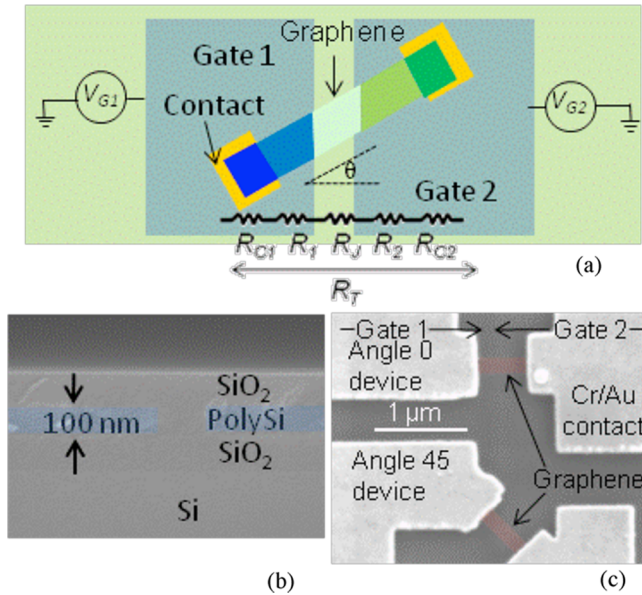
Figure 1. Graphene p−n junctions. (a) Device schematic showing the resistance components. False-color SEM of (b) wafer cross-section (c) two graphene channels on top of the split gates with tilt angles 0 and 45°.

section; two fabricated GPNJs (oriented at angles 0 and 45° to the SG) patterned on the same exfoliated flake are shown in Figure 1c.

We measured two-terminal resistance R_T for a small fixed bias (2 mV) by sweeping SG biases V_{G1} and V_{G2} independently and in high vacuum to reduce resistance hysteresis. As measured, R_T has parasitic components from the contacts and the graphene channels on both sides of the junction. They can be subtracted from R_T to extract a two-dimensional plot of just the junction resistance, the component that is predicted to have a strong angular dependence. This is done by first considering R_T as a combination of these gate bias-dependent parasitic terms in series with the junction resistance R_J, as shown in Figure 1a

$$R_T(V_{G1}, V_{G2}) = R_{C1}(V_{G1}) + R_{C2}(V_{G2}) + R_1(V_{G1})$$
$$+ R_2(V_{G2}) + R_J(V_{G1}, V_{G2})$$

The 1 and 2 refer to SGs 1 and 2, respectively; $R_{C1, 2}$ are the contact resistances and $R_{1, 2}$ are the channel resistances. These four terms depend only on the bias of the SG and are not assumed to be symmetric about the junction. Each can be measured unambiguously in the unipolar configuration to allow the extraction of the junction resistance. Specifically, the averaged junction resistance $R_{JAV}(V_{G1}, V_{G2})$ can be found as

$$2R_{JAV}(V_{G1}, V_{G2}) = R_T(V_{G1}, V_{G2}) + R_T(V_{G2}, V_{G1})$$
$$- R_T(V_{G1}, V_{G1}) - R_T(V_{G2}, V_{G2})$$
$$= R_J(V_{G1}, V_{G2}) + R_J(V_{G2}, V_{G1})$$
$$- R_J(V_{G1}, V_{G1}) - R_J(V_{G2}, V_{G2}) \qquad (1)$$

$R_{JAV}(V_{G1}, V_{G2})$ depends only on the junction resistances for any bias combinations V_{G1} and V_{G2}. For bipolar doping ($V_{G1} \times V_{G2} < 0$), the last two terms in eq 1 are much smaller than the first two and can be neglected. Assuming symmetry in transmission, we then have $R_{JAV}(V_{G1}, V_{G2}) \simeq R_J(V_{G1}, V_{G2}) = R_J(V_{G2}, V_{G1})$ for

the bipolar case. We used eq 1 to extract $R_{JAV}(V_{G1}, V_{G2})$ from both 2-and 4-terminal total resistances (R_{2T}, R_{4T}, respectively) and obtained near-identical results (see Supporting Information). Compared to a 4-terminal device structure, a 2-terminal structure, due to the lack of additional leads for voltage measurement, allows well-defined channel widths and shorter channel lengths, both highly desirable in our experiment and analysis. Therefore, in the rest of our discussion, we focus on 2-terminal resistance measurements to extract the junction resistance $R_{JAV}(V_{G1}, V_{G2})$ using eq 1.

We first measure the transfer curves, that is, the total device resistance as a function of uniform channel doping, achieved by sweeping V_{G1} and V_{G2} together, from which we extract mobility and n_0, a parameter that characterizes the average hole−electron density at the DP, using the model of Kim et al.[16] Next, we sweep V_{G1} and V_{G2} independently to find the doping-dependent total resistance $R_T(V_{G1}, V_{G2})$. In Figure 2 insets, we
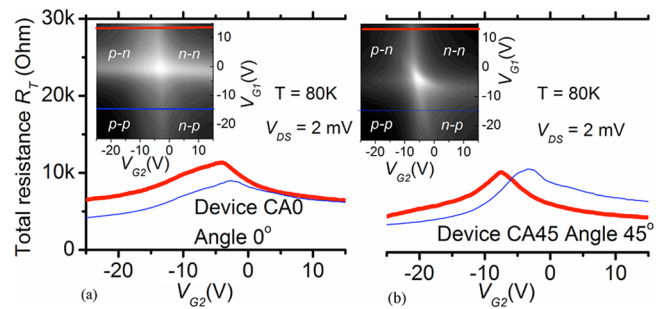

Figure 2. Two-terminal resistance of graphene channels (CVD-grown, on hBN flakes) at tilt angles (a) 0 and (b) 45° to the junction normal. Insets show R_T as grayscale plots of the SG biases V_{G1} and V_{G2}, the main panels show the dependence on V_{G2} for constant V_{G1}, the traces mapped to cuts in the insets.

show $R_T(V_{G1}, V_{G2})$ as two-dimensional grayscale plots for two graphene channels, patterned on CVD-grown graphene transferred onto hBN surfaces (Figure S6 in the Supporting Information shows the electrical transfer curves). The two channels have identical dimensions ($L = 0.5 \mu m$, $W = 0.3 \mu m$), but make 0 and 45° to the SG. The gray scale plots are divided into four quadrants made up of unipolar (p−p, n−n) and bipolar (n−p, p−n) junctions based on the polarities of V_{G1} and V_{G2} with respect to the Dirac point. The main plots in Figure 2 show the dependence of R_T on V_{G2} for constant V_{G1}, mapped to the traces in the grayscale plots. These traces show the characteristic resistance asymmetry between unipolar and bipolar doping configurations that has been observed by others.[17,18] In a two terminal configuration, however, the origin of the asymmetry cannot be determined from R_T alone as it includes the channel and contact resistances, which themselves may be asymmetric.[19,20] To unambiguously measure the junction resistance, we subtract the parasitic components from R_T to obtain R_{JAV}, using the procedure described earlier. The resulting two-dimensional gray scale plots of R_{JAV} are shown in the insets of Figure 3 for the same two devices shown in Figure 2, plotted as a function of the doping relative to the DP. After the parasitic terms are removed, the four quadrants are demarcated more clearly than those for R_T in Figure 2 as R_{JAV} for unipolar junctions are small because of the near exact cancellation of terms in eq 1 for most doping ranges. The solid and dashed line traces in the main plot of Figure 3 show the variations of R_{JAV} on the symmetric doping line, $V_{G1} - V_{DP} =$
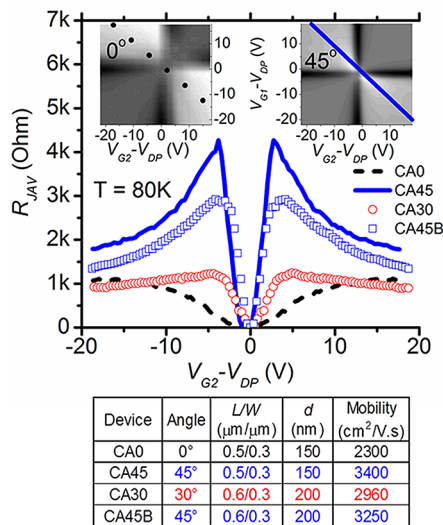
Figure 3. Extracted junction resistance R_{JAV} for the 0 and 45° tilt GPNJs shown in Figure 2. (Insets) R_{JAV} as grayscale plots of the doping levels, main panel: R_{JAV} as functions of symmetric doping levels $V_{G1} - V_{DP} = -(V_{G2} - V_{DP})$, mapped to the diagonal cuts in the inset. The traces with markers are for two additional GPNJs from the same sample with tilts 30 and 45°, the table lists all GPNJ parameters.

Device	Angle	L/W (μm/μm)	d (nm)	Mobility (cm²/V.s)
CA0	0°	0.5/0.3	150	2300
CA45	45°	0.5/0.3	150	3400
CA30	30°	0.6/0.3	200	2960
CA45B	45°	0.6/0.3	200	3250

$-(V_{G2} - V_{DP})$, mapped to the diagonal traces in the insets. For comparison, R_{JAV} for two additional GPNJs from the same sample with angles 30 and 45° are also plotted (markers); the junction parameters are listed in Figure 3. For the 45° junctions, R_{JAV} is significantly larger and has a distinctive peak at low doping ranges, which is much reduced or absent for the 0 and 30° junctions. The trend is further supported by data from a second set of GPNJs made on exfoliated graphene, shown in Figure 4. For brevity, we show only the junction
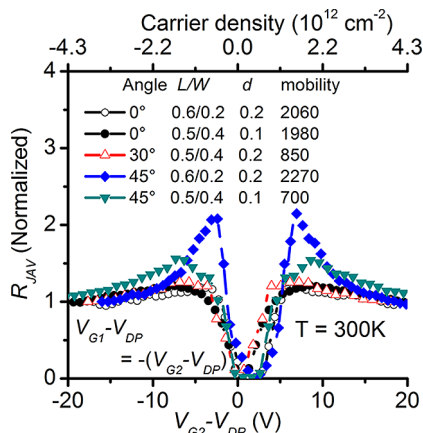
Figure 4. Normalized GPNJ resistance R_{JAV} for mechanically exfoliated GPNJs for different tilt angles. The unit in the legend is micrometers for length and cm²/(V s) for mobility.

resistances, extracted using the same procedure as the CVD GPNJ in Figure 3. Here too, a pronounced resistance peak for the 45° tilt junctions, similar to Figure 3, is observed. Because of a wider distribution in channel width and mobility for the second set (listed in Figure 4) the junction resistances also have a commensurately larger distribution, and for clarity they have been normalized to the resistances at the highest symmetric doping levels. At high doping levels, a large number of

momentum modes are supported and the angular dependence becomes less pronounced, so normalizing in this way preserves the essential features seen at low doping.

From the dependence of R_{JAV} with the junction parameters we examined (listed in Figures 3 and 4), we can exclude that the resistance peaks are from diffusive contribution due to the geometrical differences introduced by the tilt. For the 45° junction, carriers have to traverse a longer distance than in the 0° junction and could contribute to a higher diffusive resistance of at most a factor of 1/cos (45°) = 1.41. However, the near identical resistances for the two 0° junctions in Figure 4, where the junction spacing d is changed by a factor of 2, rule out this possibility. A similar result is observed for the two 45° junctions in Figure 3, where the resistance peaks are relatively unaltered with the change in d; these curves in fact almost coincide when normalized at high doping (not shown). Also, the increase in the local resistivity in bipolar junctions, where the carrier density compared to unipolar junctions is lower at all points inside the junction, should result in a scaling of the resistances at all doping levels and tilt angles, which we do not observe and thus cannot ascribe the resistance peaks to a scaling factor.

Instead, the main factors enhancing the angular dependence seem to be carrier mobility and geometric width. For the two 45° junctions in Figure 4, a higher peak height is observed for the junction with higher mobility (larger mean free path) and smaller width (fewer transverse modes), which points toward contribution from ballistic effects to the resistance. This is corroborated by our analysis of R_{JAV} in the ballistic limit, that we provide below.

To quantify the differences in R_{JAV} with angle, we first calculate the junction conductance in the ballistic limit, noting that a treatment in the purely diffusive limit cannot account for the angular dependence we observe. A similar conclusion was drawn in[11] for the study of Klein tunneling in the zero angle case. Our calculation is further aided by the analysis of Fogler[21,22] that uses the dimensionless parameter $\beta \equiv n'(e/\mu h)^{-3/2}$ with n' being the carrier density gradient to distinguish between ballistic and diffusive transport regimes in a GPNJ. Here, β gives a measure of the effective junction length compared to the carrier mean path and has been used to understand experimental data.[11] The ballistic contribution becomes appreciable at $\beta = 1$ and progressively dominates with increasing β. For $\mu \geq 2000$ cm²/(V s), typical for the GPNJ shown in Figures 3 and 4, β was found to exceed 1 for SG biases $V_{G1,2} > 2$ V, a range that includes the R_{JAV} peaks, and in fact exceeded 5 when averaged for the whole bias range, which suggests that it is reasonable to expect ballistic contribution to the GPNJ resistance.[11,21]

Within the Landauer formulation in the ballistic limit, the junction conductance is calculated by summing the contribution from all the modes. Here, we explicitly include the temperature dependence to compare to our experimental results. We thus have $G = ((4e^2)/h) \int_{-\infty}^{\infty} \Sigma_{M(E)} T(M) [-(\partial f/\partial E)] dE$, where f is the Fermi function, $M(E)$ are the modes at energy E and $T(M)$ is the transmission coefficient for a given mode. The prefactor 4 accounts for spin and valley degeneracy in graphene. For symmetric unipolar junctions, $T = 1$ for all modes, independent of angle. For bipolar junctions at tilt angle $\alpha = 0$, T is an exponentially decaying function of the incidence angle[7] for which the conductance can be written as

$$G_{\text{pn}} = \frac{4e^2}{h} \int_{-\infty}^{\infty} dE \left(-\frac{\partial f}{\partial E} \right) \sum_{m=-N(E)}^{N(E)} e^{-\sqrt{\pi} d(k_m)^2 / (\hbar v(|\mathbf{k}_{F1}| + |\mathbf{k}_{F2}|))}$$

$$(2)$$

where the sum is over the transverse momentum modes $k_m = 2\pi m/w$, quantized due to the finite channel width, $N(E) = \text{int}[(E/\hbar v)(w/2\pi)]$ is the maximum allowed value of m at a given energy, $\mathbf{k}_{F1}$, $\mathbf{k}_{F2}$ are the Fermi wave vectors on both sides of the junction, and $v \approx 10^6 \text{cm/s}$ for graphene. The construction of eq 1 uses the expression for T in reference,[7] derived for $\alpha = 0$ using the fact that k_m is conserved across the junction as there is no electric field in the transverse direction.[7] Tilting the graphene channel by $\alpha \neq 0$ changes the incidence angle of all the modes, and the transverse momenta in eq 2 now need to be rereferenced with respect to the electric field normal to the junction, for which the conductance can be written as

$$G_{\text{pn}}(\alpha) = \frac{4e^2}{h} \int_{-\infty}^{\infty} dE \left(-\frac{\partial f}{\partial E} \right)$$
$$\sum_{m=-N(E)}^{N(E)} e^{-\sqrt{\pi} d(k'_m(\alpha))^2 / \cos(\alpha)(\hbar v(|\mathbf{k}_{F1}| + |\mathbf{k}_{F2}|))}$$

$$(3)$$

where $k'_m(\alpha) = (E/\hbar v)\sin(\sin^{-1}\{[(2\pi m)/w][(\hbar v)/E]\} + \alpha)$, reflecting the change in the transverse momentum due to the shift α in the incidence angle of any momentum mode. The factor $1/\cos(\alpha)$ accounts for the increased travel distance for a junction at an angle. Setting $\alpha = 0$ results in the same expression given in eq 2. The above formulations for the GPNJ resistance assume that the carrier density in the GPNJ varies smoothly in the junction and crosses zero somewhere inside the junction, which is not realized in practice due to the presence of impurities-induced electron−hole puddles when the Fermi level is near the DP.[23] Our calculation is thus strictly valid in cases where the external doping levels are significantly higher than the average electron−hole density at the MCP, a measure of which can be found from the parameter n_0. We estimate n_0 using the model of[16] for our graphene to range from 2 to 8 × 10^{11} cm^{-2}, a significant fraction of the doping range we examined, but consistent with $\mu n_0 = 1.15 \times 10^{15}$ V/s reported by Chan et al.[24] For $n_{1,2} < n_0$ the externally induced carrier density is not significant enough to create a well-defined p−n junction. In the absence of a p−n junction, it is more reasonable to consider diffusive transport as the relevant transport length is the contact-to-contact separation (∼0.5 μm), which is about 10 times the estimated mean free path (MFP)[25] for our channels. On the other hand, for $n_{1,2} > n_0$, as there is scattering at the p−n junction created by the SG, the relevant transport length is the contact-to-junction separation which, considering the finite SG spacing of ∼0.15 μm, is only about 3 times the MFP. Thus n_0 becomes our demarcation point above which ballistic contribution to transport is considered.

To compare to our experimental results, we calculate the junction resistance for two symmetrically doped GPNJs with angles 0 and 45° in Figure 5. We use $d = W = 200$ nm, and plot for different values of n_0; for $n_{1,2} \geq n_0$, R_{JAV} is calculated using ballistic resistances as described above; for $n_{1,2} < n_0$ we estimate the resistance as $\{[(We\mu \cos \alpha)/d]n_{\text{av}}\}^{-1}$ for a carrier density n_{av} averaged from n_0 and a linear profile for the externally induced density $n(x)$ in the junction.

The central features in the calculated R_{JAV} shown in Figure 5 follow the doping dependence as observed in our data. For the
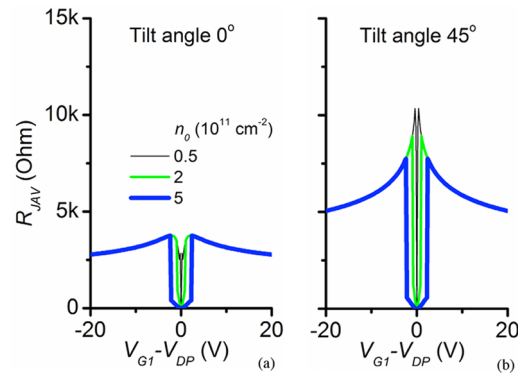
Figure 5. Calculated R_{JAV} at $T = 300$ K for (a) 0 and (b) 45° tilted GPNJs ($W = d = 200$ nm) as a function of the p−n doping levels $V_{\text{G1}} - V_{\text{DP}} = -(V_{\text{G2}} - V_{\text{DP}})$, for different average background doping levels (n_0).

45° junction, a sharp peak is observed at low doping that is not present in the 0° junction, similar to our experimental results. At low doping, a large fraction of the momentum modes is nearly aligned along the graphene channel, and it largely determines the junction resistance. For the 0° angle junction, these modes result in significant transmission, including Klein tunneling, as seen in Figure 5a. On the other hand, for the 45° junction the incidence angle for the same modes is nearly 45°, resulting in a significantly lower transmission probability and a peak in the resistance as seen in Figure 5b. For both junctions, increasing the doping results in a larger number of momentum modes and a denser distribution of incidence angles, reducing the junction resistance. For $n_{1,2} < n_0$, the junction resistance is significantly lower, typical of diffusive resistances compared to ballistic[17] and varies only by the geometrical factor cos 45° between the junctions.

Finally, we discuss effects not accounted for in our model that may explain the discrepancy in the magnitude of resistance between our calculated and measured results. First, the lower values of the measured resistances suggest that a contribution from diffusive transport must be included to explain the measured resistances for n_1, $n_2 > n_0$, although the exact contributions from ballistic and diffusive transport are not yet fully understood. Another reason for the higher calculated values for R_{JAV} could be the subtraction of an underestimated ballistic $R_J(n_1, n_1)$ with the assumption $T = 1$, as additional unipolar junction scattering[10] may be possible in the junction if $n(x)$ across the GPNJ differs from n_1 on the SG. Despite the difference in magnitude, the relative height of the 45° R_{JAV} peak (≈2.5, normalized) is in good agreement with calculation. This may be explained by the possible enhancement of the peak in experiment due to some degree of carrier collimation along the channel introduced by the contacts,[26] which may allow transmission of only near-normal-incident carriers, an effect not taken into account in the calculation.

In conclusion, we have fabricated graphene p−n junctions with buried gates and studied the angle-dependent transport by measuring the resistance of individual graphene junctions. We have examined two sets of junctions made on graphene obtained from exfoliation and CVD-growth techniques, both of which show a peak in the junction resistance at low doping that becomes more pronounced as the channel is tilted relative to the junction. These features are reproduced in our calculations based on the theoretical incidence angle-dependence of

transmission and suggest a significant component from ballistic carriers to the junction resistance.

■ ASSOCIATED CONTENT

Ⓢ Supporting Information

Comparison of junction resistances extracted from 2 and 4-terminal measurements; device resistance in the case of uniform channel doping. This material is available free of charge via the Internet at http://pubs.acs.org.

■ AUTHOR INFORMATION

Corresponding Author
*E-mail: (S.S.) ssutar@albany.edu; (J.U.L.) jlee1@albany.edu.

Notes
The authors declare no competing financial interest.

■ ACKNOWLEDGMENTS

■ REFERENCES

(1) Castro Neto, A. H.; Guinea, F.; Peres, N. M. R.; Novoselov, K. S.; Geim, A. K. The electronic properties of graphene. *Rev. Mod. Phys.* **2009**, *81*, 109−162.

(2) Adam, S.; Hwang, E. H.; Galitski, V. M.; Das Sarma, S. A self-consistent theory for graphene transport. *Proc. Natl. Acad. Sci. U.S.A.* **2007**, *104*, 18392−18397.

(3) Das Sarma, S.; Adam, S.; Hwang, E. H.; Rossi, E. Electronic transport in two-dimensional graphene. *Rev. Mod. Phys.* **2011**, *83*, 407−470.

(4) Beenakker, C. W. J. *Colloquium*: Andreev reflection and Klein tunneling in graphene. *Rev. Mod. Phys.* **2008**, *80*, 1337−1354.

(5) Rossi, E.; Bardarson, J. H.; Brouwer, P. W.; Das Sarma, S. Signatures of klein tunneling in disordered graphene *p-n-p* junctions. *Phys. Rev. B* **2010**, *81*, 121408.

(6) Cheianov, V. V.; Fal'ko, V.; Altshuler, B. L. The focusing of electron flow and a Veselago lens in graphene p-n junctions. *Science* **2007**, *315*, 1252−1255.

(7) Cheianov, V. V.; Fal'ko, V. I. Selective transmission of Dirac electrons and ballistic magnetoresistance of *n-p* junctions in graphene. *Phys. Rev. B* **2006**, *74*, 041403.

(8) Low, T.; Appenzeller, J. Electronic transport properties of a tilted graphene *p-n* junction. *Phys. Rev. B* **2009**, *80*, 155406.

(9) Sajjad, R.; Ghosh, A. High efficiency switching using graphene based electron "optics". *Appl. Phys. Lett.* **2011**, *99*, 123101.

(10) Williams, J. R.; Lundstrom, M. S.; Low, T.; Marcus, C. M. Gate-controlled guiding of electrons in graphene. *Nat. Nanotechnol.* **2011**, *6*, 222.

(11) Stander, N.; Huard, B.; Goldhaber-Gordon, D. Evidence for klein tunneling in graphene *p-n* junctions. *Phys. Rev. Lett.* **2009**, *102*, 026807.

(12) Young, A. F.; Kim, P. Quantum interference and klein tunneling in graphene heterojunctions. *Nat. Phys.* **2009**, *5*, 222−226.

(13) Li, X.; et al. Large-area synthesis of high-quality and uniform graphene films on copper foils. *Science* **2009**, *324*, 1312−1314.

(14) Dean, C. R.; et al. Boron nitride substrates for high-quality graphene electronics. *Nat. Nanotechnol.* **2010**, *5*, 722−726.

(15) Gannett, W.; et al. Boron nitride substrates for high mobility chemical vapor deposited graphene. *Appl. Phys. Lett.* **2011**, *98*, 242105.

(16) Kim, S.; et al. Realization of a high mobility dual-gated graphene field-effect transistor with Al_2O_3 dielectric. *Appl. Phys. Lett.* **2009**, *94*, 062107.

(17) Huard, B.; et al. Transport measurements across a tunable potential barrier in graphene. *Phys. Rev. Lett.* **2007**, *98*, 236803.

(18) Gorbachev, R. V.; et al. Conductance of p-n-p Graphene Structures with Air-Bridge Top Gates. *Nano Lett.* **2008**, *8*, 1995−1999.

(19) Huard, B.; Stander, N.; Sulpizio, J. A.; Goldhaber-Gordon, D. Evidence of the role of contacts on the observed electron-hole asymmetry in graphene. *Phys. Rev. B* **2008**, *78*, 121402.

(20) Chiu, H-Y; Perebeinos, V.; Lin, Y-M; Avouris, P. Controllable p-n Junction Formation in Monolayer Graphene Using Electrostatic Substrate Engineering. *Nano Lett.* **2010**, *10*, 4634−4639.

(21) Fogler, M. M.; Novikov, D. S.; Glazman, L. I; Shklovskii, B. I. Effect of disorder on a graphene *p-n* junction. *Phys. Rev. B* **2008**, *77*, 075420.

(22) Zhang, L. M.; Fogler, M. M. Nonlinear screening and ballistic transport in a graphene *p-n* junction. *Phys. Rev. Lett.* **2008**, *100*, 116804.

(23) Martin, J.; et al. Observation of electron-hole puddles in graphene using a scanning single-electron transistor. *Nat. Phys.* **2008**, *4*, 144−148.

(24) Chan, J.; et al. Reducing Extrinsic Performance-Limiting Factors in Graphene Grown by Chemical Vapor Deposition. *ACS Nano* **2012**, *6*, 3224−3229.

(25) Bolotin, K. I.; et al. Ultrahigh electron mobility in suspended graphene. *Solid State Commun.* **2008**, *146*, 351.

(26) Mueller, T.; et al. Role of contacts in graphene transistors: A scanning photocurrent study. *Phys. Rev. B* **2009**, *79*, 245430.